Cu–ZnO Core–Shell Structures for CO2 Hydrogenation to Methanol: Insights into Reactivity and Deactivation under High-Pressure Conditions

Gaikwad, Rohit; Kränzlin, Niklaus; Benet-Buchholz, Jordi; Niederberger, Markus; Koziej, Dorota; Urakawa, A.

DOI
10.1021/acs.energyfuels.5c03664

Publication date
2025

Document Version
Final published version

Published in
Energy & Fuels

Citation (APA)
Gaikwad, R., Kränzlin, N., Benet-Buchholz, J., Niederberger, M., Koziej, D., & Urakawa, A. (2025). Cu–ZnO Core–Shell Structures for CO2 Hydrogenation to Methanol: Insights into Reactivity and Deactivation under High-Pressure Conditions. *Energy & Fuels*, *39*(46), 22342-22355. https://doi.org/10.1021/acs.energyfuels.5c03664

energy&fuels

pubs.acs.org/EF
Article

Cu−ZnO Core−Shell Structures for CO_2 Hydrogenation to Methanol: Insights into Reactivity and Deactivation under High-Pressure Conditions

Published as part of Energy & Fuels special issue "2025 Pioneers in Energy Research: Rose Amal".

Rohit Gaikwad, Niklaus Kränzlin, Jordi Benet-Buchholz, Markus Niederberger, Dorota Koziej, and Atsushi Urakawa*

Cite This: *Energy Fuels* 2025, 39, 22342−22355

ABSTRACT: Methanol is a valuable chemical energy carrier and C1 feedstock, with significant research efforts directed toward its production via CO_2 hydrogenation. Here, we report a surfactant-free, non-aqueous synthesis of Cu−ZnO core−shell catalysts (Cu_2O core and ZnO shell), featuring uniform morphology and high performance. This enables a better understanding of the Cu−ZnO synergy, providing insights into the formation of highly active and selective sites as well as catalyst stability. The optimal core−shell catalyst achieved 53% CO_2 conversion and 84% methanol selectivity. Comprehensive characterization, including *operando* X-ray diffraction at 184−331 bar reactant pressure, was performed on both the core−shell material and a commercial $Cu/ZnO/Al_2O_3$ catalyst, before and after the reaction. The results revealed that the highly active state of the catalyst promotes the carbonation of ZnO, leading to the formation of $ZnCO_3$ during the reaction. This is likely driven by the acidic reaction medium formed from the dissolution of CO_2 in water under high conversion conditions. While $ZnCO_3$ formation may contribute to catalyst deactivation, it could also offer a rigid structure that supports highly active and selective, dispersed Cu−Zn interactions.

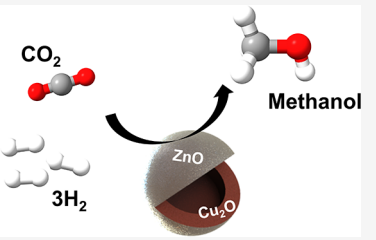

1. INTRODUCTION

The Industrial Revolution and modern lifestyles have increased fossil fuel use, causing significant carbon dioxide (CO_2) emissions. Converting CO_2 into useful chemicals or fuels is a key approach to address excess CO_2 and reduce fuel demand. Methanol, a sustainable liquid fuel, can be produced through CO_2 hydrogenation.[1−4]

$$CO_2 + 3H_2 = CH_3OH + H_2O$$
$$\Delta H = -49.43\ \text{kJ mol}^{-1} \quad (1)$$

As shown above, eq 1 is an exothermic reaction. According to Le Chatelier's principle, CO_2 hydrogenation at high pressure and low temperature promotes methanol formation, in particular when the reaction reaches equilibrium.[3,5−7] Recent developments in renewable hydrogen production make this high-pressure process both economically and technically more feasible.[1,3,8−11]

Copper (Cu)-based catalysts, particularly when mixed with zinc oxide (ZnO), are widely studied for their high catalytic activity in methanol synthesis from carbon oxides and hydrogen under elevated pressure and temperature.[12−16] Numerous studies debate the nature of the active centers in Cu/ZnO systems and other supported Cu catalysts and elucidate the role of oxide supports.[12,17−22] While early studies indicated that Cu(0) and Cu(+1) are the active sites,[23−25] more recent experimental work[26−29] and density functional theory (DFT) calculations[30−35] suggest that various copper surfaces, such as Cu(111) and Cu(211), are highly active and selective for methanol formation. Additionally, smaller copper particle sizes and higher surface areas improve catalytic performance, but nanoparticle agglomeration during reaction processes remains a challenge.[32,36] Although Cu can independently catalyze CO_2 hydrogenation, its activity is significantly enhanced through interaction with ZnO.[32,37,38] ZnO contributes to maintaining a high dispersion of Cu particles.[39] Therefore, the Cu particle size and surface area alone are insufficient, and the presence of ZnO is necessary to stabilize intermediates and facilitate key reaction steps at the metal−oxide interface.[27,40,41] The synergistic effect between Cu and ZnO is widely recognized as a critical factor in catalyst efficiency.[17,21,29,40,42−48] More recent *operando* studies by Beck et al. showed that the Cu−ZnO interface undergoes structural

Received: July 15, 2025
Revised: October 26, 2025
Accepted: October 28, 2025
Published: November 6, 2025

https://doi.org/10.1021/acs.energyfuels.5c03664
Energy Fuels 2025, 39, 22342−22355

rearrangements that enhance the formation of active intermediates.[49,50]

Commonly, Cu−ZnO-based catalysts (alternatively written as Cu/ZnO) are synthesized via co-precipitation or impregnation methods and incorporate several components, including structural promoters. These synthesis techniques are simple and scalable, but they often lead to thermally unstable catalysts susceptible to sintering and catalyst deactivation.[51] ZnO acts as a physical spacer that mitigates Cu sintering and serves as a reservoir for atomic hydrogen, thereby facilitating hydrogen spillover to Cu.[30] Furthermore, ZnO can operate as a co-catalyst, supporting active formate formation at the Cu/ZnO interface.[52−54] Importantly, the long-term activity and deactivation of the Cu−ZnO catalyst is a well-known challenge, often attributed to the structural change of the catalyst caused by water, which is more prominent in CO_2 hydrogenation to methanol in comparison to syngas (CO + H_2) to methanol (in practice CO_2 is added or formed via a water−gas shift) as H_2O is produced from the CO_2 hydrogenation.[55−63] Water is known to accelerate sintering[41] as well as induce kinetic inhibition.[64] In this context, adopting a Cu−ZnO core−shell morphology could offer a well-defined metal−oxide interface, enhancing interaction and protecting the Cu core from sintering.[46,65,66]

Core−shell nanomaterial synthesis has gained attention for its ability to encapsulate central metal particles,[67−69] possibly preventing agglomeration and enhancing stability even under extreme conditions. Unlike traditional high-temperature methods, advanced approaches, such as non-aqueous sol−gel synthesis, enable precise control over nanostructures at lower temperatures, producing stable, pure, and homogeneous materials.[70] This method addresses challenges of aqueous processes by using organic solvents, which aid in controlling the particle size, shape, surface, and composition.[71] Non-aqueous, surfactant-free synthesis is preferred due to concerns about nanoparticle toxicity associated with surfactants. Metal oxide precursors, like acetates, acetylacetonates, and alkoxides, are used with various solvents; however, metal halides can introduce impurities.[72,73] Therefore, alternative precursors are often selected for improved purity.

In this work, a straightforward method for synthesizing Cu−ZnO core−shell nanomaterials via non-aqueous sol−gel synthesis was developed, offering advantages of high purity, tunability, and low synthesis temperatures,[70,73] as a model system to gain insights into the Cu−ZnO interfaces. Benzyl alcohol served as the reducing agent,[74,75] and the resulting core (Cu component)−shell (Zn component)-structured materials were tested for high-pressure CO_2 hydrogenation to methanol, yielding insights into the Cu−ZnO synergies. Structural changes in the Zn shell and their effects on the reaction were investigated using X-ray diffraction (XRD). The relevance of the findings on the Zn structure was verified using the commercial Cu/ZnO/Al_2O_3 catalyst by high-pressure *operando* XRD at 200−360 bar (reactant pressure of 184−331 bar).

2. EXPERIMENTAL SECTION

2.1. Chemicals. All the chemical reagents were used as purchased from Sigma-Aldrich. Copper(I) acetate (Sigma-Aldrich, 97%), zinc acetate (Sigma-Aldrich, 99.99%), and benzyl alcohol (Sigma-Aldrich, puriss) were used as received. The reactant gas mixture (CO_2/H_2/Ar = 23:69:8) was purchased from Abelló Linde (Spain).

2.2. Catalysis Synthesis. Zinc acetate and copper acetate were dissolved in benzyl alcohol in an inert atmosphere using a standard Schenk line and flask. In a typical synthesis, 5.7 mmol of zinc acetate was first dissolved in 30 mL of benzyl alcohol, and afterward, 2.5 mmol of copper acetate was added to the solution under constant stirring under N_2 flow. The reaction vessel was purged with N_2 and sealed, and the solution was further stirred for 5 min. Later, the vessel was dipped into an oil bath preheated at 160 °C under stirring for 30 min. Precipitates were separated from the liquid phase by centrifugation and washed 3 times with ethanol. Cu_2O and ZnO were also synthesized separately using an identical procedure but using only one of the precursors. The final dried powders of Cu_2O and ZnO were mixed, and this is called a "physical mixture". Also, in order to evaluate the effects of stirring on the resulting material, Cu−ZnO material was prepared by the same protocol but without stirring. Finally, these materials were dried in an oven at 80 °C, pressed, crushed, and sieved to a particle size fraction (100−300 μm) for catalytic activity tests.

2.3. Catalyst Characterization. *Ex situ* XRD patterns of all catalysts after reaction were recorded on a Bruker AXS D8 advance diffractometer equipped with a Cu tube, Ge(111) incident beam monochromator (λ = 0.1541 nm), and Vantec-1 PSD operated in transmission mode. Data were recorded in 20−80° 2θ with a step size of 0.02° and a counting time of 4 s per step. The phases were confirmed using the JCPDS database. *In situ* and *operando* XRD measurement details are explained in the Supporting Information. Quantitative crystalline phase analysis of Cu_2O−ZnO at different weight percent loadings before the reaction was performed using MAUD software.

H_2 temperature-programmed reduction (TPR) of the as-prepared catalyst was carried out on a Thermo TPDRO 1100 equipped with a thermal conductivity detector (TCD). The samples were heated from 25 to 400 °C at a rate of 2 °C min^{-1} under a stream of 5% H_2 in N_2 at 20 mL min^{-1} flow rate. A soda lime (CaO + Na_2O) trap was used to adsorb H_2O and CO_2. N_2 isotherms at 77 K were measured on a Quantachrome Autosorb 1-MP analyzer to obtain the Brunauer−Emmett−Teller (BET) surface area. Prior to the analysis, sample was degassed in vacuum at 250 °C for 12 h.

Pulse chemisorption was used to measure the copper surface area and dispersion using nitrous oxide as reported by Evans et al.[76] The samples were reduced prior to analysis by 5% H_2 in He stream at 330 °C at 2 °C heating rate and held for 3 h. The samples were cooled down to 90 °C under He flow. For analysis, a known volume of N_2O was then injected as a pulse by using a six port valve. N_2O at the outlet was decomposed to N_2, and then N_2 was measured by calibrated gas chromatography. Copper surface areas were calculated assuming 1.46×10^{19} copper atoms per m^2.[76] High-resolution transmission electron microscopy (HR-TEM) images were recorded on a JEOL JEM-2200FS microscope operated at 200 kV. Energy-dispersive X-ray (EDX) analyses were carried out on a FEI Talos F200X microscope operated at 200 kV in scanning transmission electron microscopy (STEM) mode. The samples for TEM analyses were dispersed in ethanol and drop-casted onto nickel-coated copper and a nickel grid and measured by JEOL 1011. In the case of scanning electron microscopy (SEM) analysis, the samples were ultrasonicated in ethanol for 10 min prior to measurement using a JEOL 6400.

2.4. Catalytic Test. Carbon dioxide hydrogenation to methanol was studied in a high-pressure continuous flow fixed-bed stainless-steel reactor (1.8 mm inner diameter). The details of the high-pressure fixed-bed reactor and analytical systems are described elsewhere.[15] Briefly, a high-pressure continuous flow reactor was used for CO_2 hydrogenation to methanol. The reactor was made up of a stainless-steel tube with an outer diameter of $^1/_8$ in. and a 0.07 in. inner diameter. The varied composition catalyst was pelletized without any pretreatment. The pellets were crushed and sieved to a particle size of 100−300 μm, and 50 mg of the catalyst was charged to the reactor with the bed length of 10 mm. The catalyst was supported on quartz wool in the reactor to avoid any movement against flow under pressure. The catalyst was reduced prior to the reaction using a hydrogen stream of 20 mL min^{-1} for 2 h at 330 °C at atmospheric pressure. Later, the catalyst bed was cooled down to room temperature and pressurized using premixed reactant gas to a desired

https://doi.org/10.1021/acs.energyfuels.5c03664
Energy Fuels 2025, 39, 22342−22355

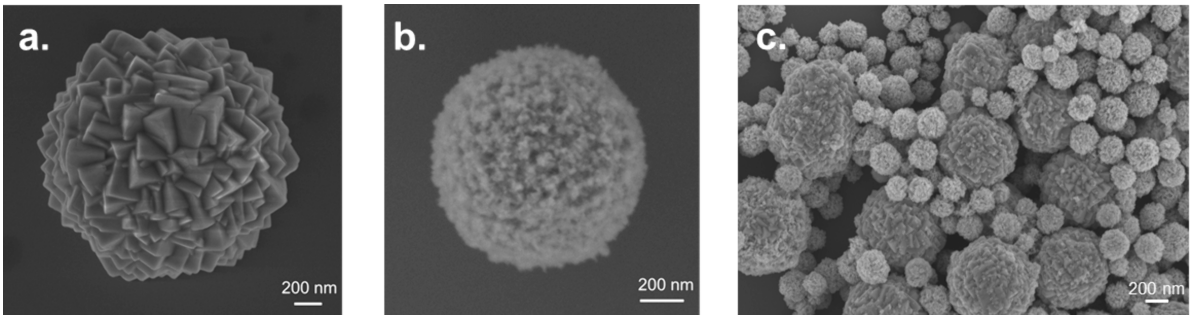

Figure 1. SEM images of the (a) Cu_2O sphere and 30 wt % Cu_2O−ZnO prepared (b) with and (c) without stirring during the synthesis.

reaction pressure. A high-pressure syringe pump (Teledyne ISCO 260D) was used to dispense the premixed reactant gases to precisely maintain the CO_2 and H_2 ratio of 1:3 at a 4000 h^{-1} gas hourly space velocity. The catalysts were tested for CO_2 hydrogenation to methanol at four different pressures of 30, 200, 360, and 480 bar (including 8% Ar in the feed as an internal standard) with the actual reactant pressure of CO_2 and H_2 of 28, 184, 331, and 442 bar, respectively. The reactor was heated to the reduction or reaction temperature at a ramp rate of 10 °C min^{-1}, and during the reaction, the temperature was maintained for at least 3 h to ensure multiple consistent gas chromatography (GC) measurements. The effluent stream was analyzed by an online GC instrument (Bruker 450) equipped with a Porapak Q + Mol sieve column and a TCD for analysis of gaseous products and a CP wax 52 CB capillary column and a flame ionization detector (FID) for analysis of methanol and other oxygenates.

3. RESULTS AND DISCUSSION

3.1. Material Structure. Figure 1 displays SEM images of materials produced via different non-aqueous sol−gel protocols (zoom-out views are also presented in Figure S8). Figure 1a shows the nanostructured material synthesized with only the Cu precursor, forming spherical cuprous oxide (Cu_2O) with cube-like constituents, as indicated by sharp edges. Figure 1b and c compares the materials synthesized in the presence of both Cu and Zn precursors, with and without stirring at a 3:7 (Cu_2O/ZnO) ratio. Stirring produces homogeneous ZnO nanoparticle coverage on Cu_2O cores, whereas without stirring, the formation appears less uniform and may involve partial phase segregation between Cu_2O and ZnO.

Figure 2 shows TEM images of the nanomaterials synthesized under stirring with the Cu content at 15, 30, 50, and 70 wt % (Figure 2a−d). In all cases, ZnO nanoparticles coat the Cu_2O core to varying degrees dependent on the Cu_2O/ZnO weight ratio. The resulting spherical nanomaterials range from 500 to 800 nm in diameter. As the Cu_2O−ZnO weight ratio decreased, ZnO nanoparticles aggregated, forming more complete and thicker ZnO layers on the Cu_2O core (Figure 2). At a lower Zn content, a thin and uneven ZnO coating appeared on Cu_2O (Figure 2d).

While ZnO is mainly distributed as a shell around the Cu_2O cores, we also observed a group of ZnO small spheres that are not directly attached to the Cu_2O core, particularly in samples with a greater ZnO content. This dispersed arrangement may be beneficial for methanol synthesis as it provides ZnO coverage that stabilizes Cu_2O against agglomeration at elevated temperatures while maintaining accessible Cu−ZnO interfacial sites. HR-TEM and EDX analyses of 30 and 70 wt % Cu_2O−ZnO materials confirmed that cores and shells are primarily composed of Cu and Zn, respectively (Figures 3 and 5). Figure 3 shows a hollow sphere for the 30 wt % sample, with EDX

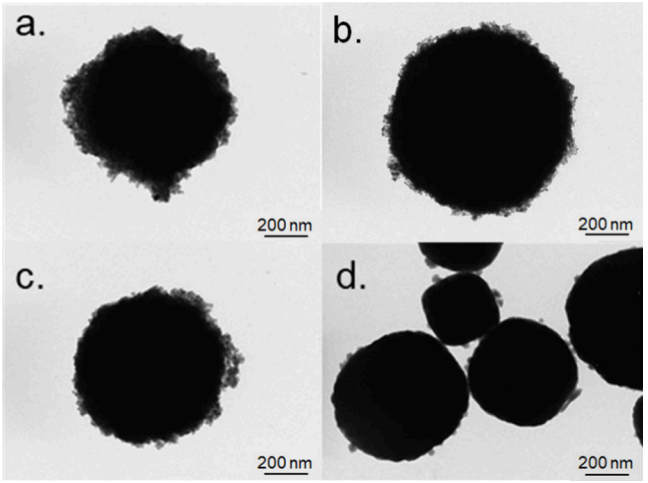

Figure 2. TEM images of (a) 15 wt %, (b) 30 wt %, (c) 50 wt %, and (d) 70 wt % (Cu_2O-basis) Cu_2O−ZnO core−shell materials.

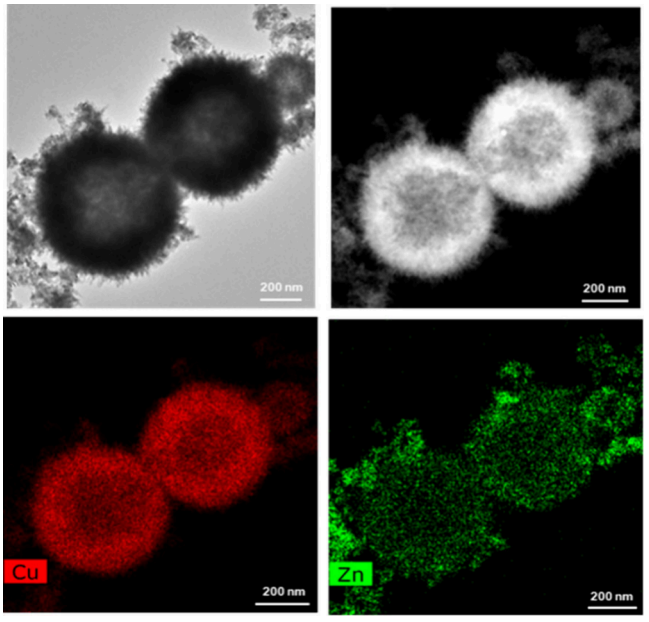

Figure 3. HR-TEM images and EDX analysis of 30 wt % Cu_2O−ZnO.

indicating partial filling of Cu_2O and uniform Zn distribution (Figure 4). In contrast, a higher Cu content (70 wt %) results in a fully filled Cu_2O core (Figure 5).

3.2. *Ex Situ* XRD. Figure 6 presents XRD patterns for materials synthesized via the non-aqueous sol−gel method, identifying two phases: Cu_2O (29.6°, 36.5°, 42.4°, 61.5°, and

https://doi.org/10.1021/acs.energyfuels.5c03664
Energy Fuels 2025, 39, 22342−22355

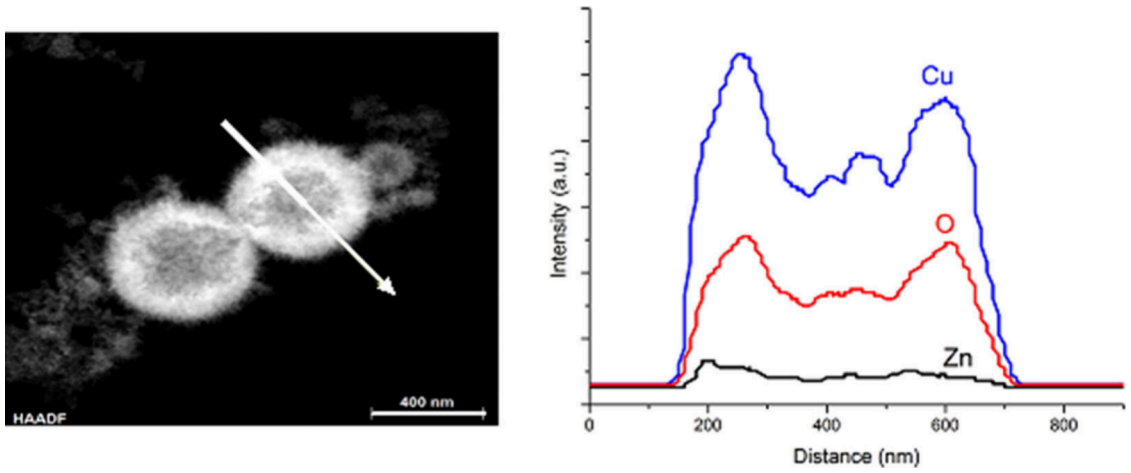

Figure 4. STEM and EDX line scan analysis of 30 wt % Cu_2O−ZnO before the reaction.

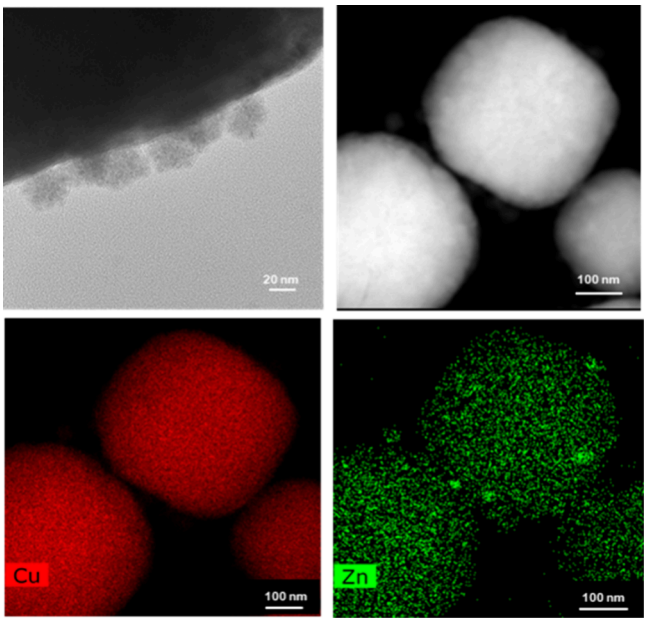

Figure 5. HR-TEM images and EDX analysis of 70 wt % Cu_2O−ZnO.

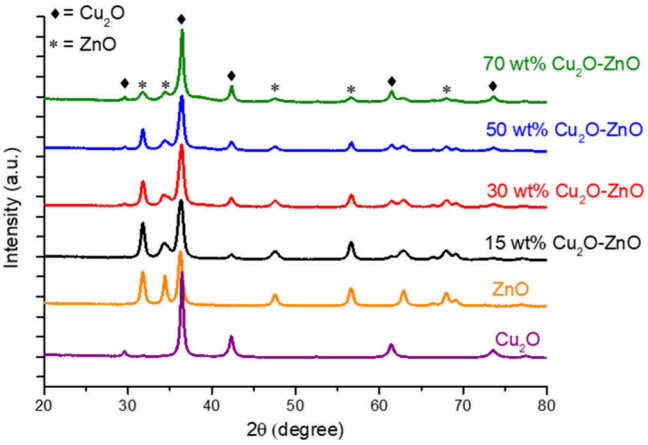

Figure 6. XRD patterns of the Cu_2O, ZnO, and Cu_2O−ZnO materials synthesized by the non-aqueous sol−gel method at varying Cu_2O−ZnO ratios.

73.6°; JCPDS 01-078-2076) and ZnO (31.8°, 34.4°, 36.2°, 47.5°, and 56.6°; JCPDS 00-036-1451). As the Cu_2O/ZnO ratio increases, Cu_2O peaks intensify and sharpen while ZnO peaks diminish. Table 1 shows that a higher Cu content generally enhances Cu_2O crystallinity, with ZnO crystallinity remaining relatively unaffected by changes in the Zn content. The XRD results confirm the phase purity of both Cu_2O and ZnO. Values represent the XRD-detectable crystalline fraction obtained by Rietveld refinement using MAUD software with COD reference structures without considering the amorphous structure contribution.

Table 1. Quantitative Crystalline Phase Analysis of Cu_2O−ZnO at Different Weight Percent Loadings before the Reaction

catalyst	Cu_2O	ZnO
Cu_2O	21	
Cu−ZnO (15 wt %)	12	15
Cu−ZnO (30 wt %)	11	16
Cu−ZnO (50 wt %)	19	19
Cu−ZnO (70 wt %)	23	13
ZnO		14

3.3. *In Situ* XRD during Thermal Treatment in H_2. Copper is highly temperature-sensitive and prone to agglomeration at elevated temperatures, which reduces its catalytic surface area. To study thermal stability and reduction behavior, XRD patterns of 30 wt % Cu_2O−ZnO were measured from 30 to 450 °C under 5% H_2/N_2 at atmospheric pressure (Figure 7). Reduction began at around 260 °C and was complete by 300 °C. Using the Scherrer equation, the Cu crystallite size increased from 12 nm (Cu_2O) to 21 nm [Cu(0), reduced at 330 °C], and further heating raised it to 23 nm, indicating strong resistance to sintering, which is common,[77] due to the ZnO shell.

3.4. H_2-TPR. H_2-TPR analysis was performed on all Cu_2O−ZnO core−shell samples and pure Cu_2O as a reference, as shown in Figure 8. Pure Cu_2O exhibited a broad reduction peak at 320 °C. With ZnO coating, the reduction profile shifted: at 30 wt % ZnO, the peak became sharper without a change in the temperature, while a higher ZnO content lowered the reduction temperature by 30−50 °C and exhibited two distinct peaks. These results indicate that ZnO, through

https://doi.org/10.1021/acs.energyfuels.5c03664
Energy Fuels 2025, 39, 22342−22355

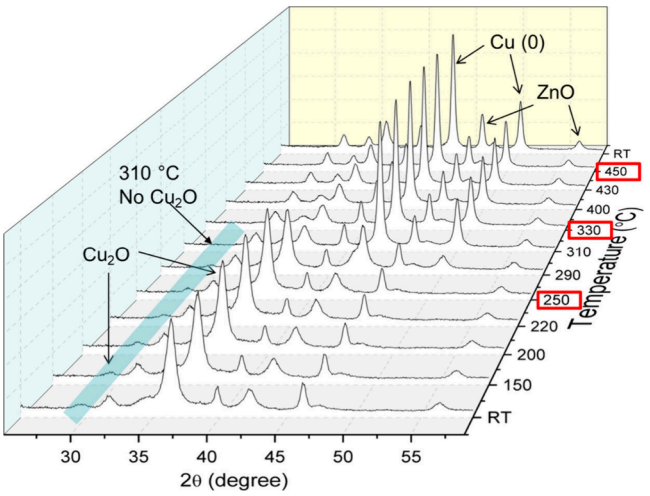

Figure 7. *In situ* XRD of 30 wt % Cu_2O−ZnO during reduction treatment with 5% H_2 in N_2 atmospheric pressure at 30−450 °C. The three temperatures in red boxes indicate three representative temperatures: before Cu_2O reduction (250 °C), when the reduction was just completed (330 °C), and after thorough reduction (450 °C).

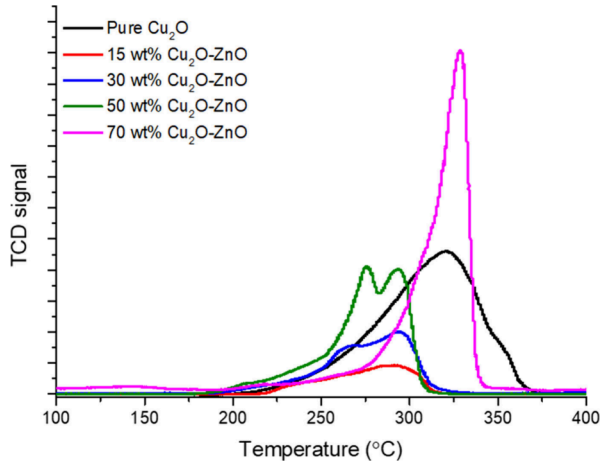

Figure 8. H_2-TPR of Cu_2O and 15, 30, 50, and 70 wt % Cu_2O−ZnO.

interaction with Cu_2O, enhances Cu_2O reducibility,[78] i.e., a factor potentially advantageous for CO_2 hydrogenation to methanol.

3.5. Catalyst Evaluation: Effects of the Cu−Zn Ratio. The catalytic performance of the Cu−ZnO core−shell materials (hereafter referred to as Cu−ZnO instead of Cu_2O−ZnO, as the materials are pre-reduced) was assessed under high-pressure conditions across a broad temperature range (220−340 °C; Figure 9). Notably, the four core−shell compositions exhibited distinct differences in both the CO_2 conversion and methanol selectivity. Overall, the CO_2 conversion showed a monotonic increase with the temperature. In contrast, trends in methanol selectivity varied significantly depending on material composition. For instance, 50 wt % Cu−ZnO demonstrated a steady rise in methanol selectivity, whereas 70 wt % Cu−ZnO displayed a consistent decrease. The 15 and 30 wt % Cu−ZnO samples exhibited an initial decline followed by a marked increase in methanol selectivity as the temperature increased.

The catalyst containing the highest copper content (70 wt % Cu−ZnO) produced the lowest CO_2 conversion, despite showing the highest methanol selectivity at lower temperatures. A reduction in the Cu content to 50 wt % resulted in a substantial enhancement in catalytic activity, accompanied by a reversal in methanol selectivity behavior, with an initial drop followed by a steady increase with the rising temperature. When the Zn content was further increased (30 wt % Cu−ZnO), the highest CO_2 conversion below 320 °C was achieved. The methanol selectivity initially decreased and then dramatically shifted from CO to methanol between 260 and 280 °C as the reaction temperature rose. This switch in the product selectivity may be caused by the insufficient hydrogen activation to drive the reaction to methanol,[34] or the highly reactive sites[49] were not yet formed at the temperature in the first catalytic test (*vide infra* for further discussion, Figure 20). For the sample with the highest Zn content (15 wt % Cu−ZnO), catalytic activity remained high and the methanol selectivity trend persisted with a pronounced decline followed by a gradual increase at elevated temperatures.

The Cu surface areas were 7.7, 10.6, 5.2, and 1.2 $m^2\ g^{-1}$ for 15, 30, 50, and 70 wt % Cu−ZnO, respectively. While this accounts for the lower catalytic activity observed with the 70 wt % Cu−ZnO sample, it does not fully explain the distinctive

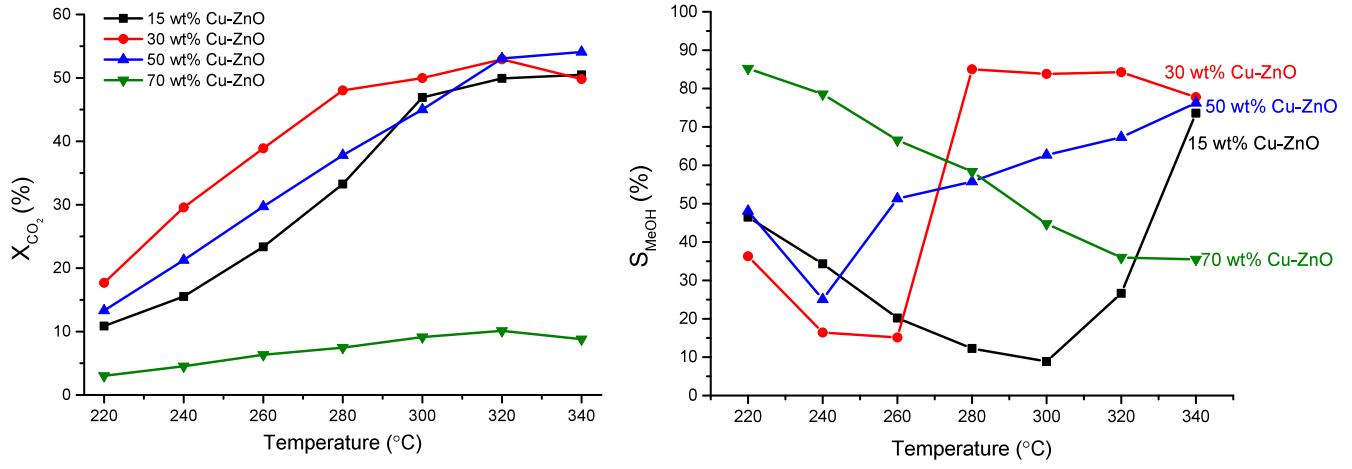

Figure 9. Effect of the reaction temperature and composition of Cu−ZnO on CO_2 conversion (left) and methanol selectivity (right) at CO_2/H_2 = 1:3, 4000 h^{-1}, and 331 bar (reactant pressure; 360 bar including Ar). Prior to the reaction, the materials were reduced to H_2 at 330 °C.

https://doi.org/10.1021/acs.energyfuels.5c03664
Energy Fuels 2025, 39, 22342−22355

selectivity patterns observed. These results suggest that the Cu−ZnO interfaces likely play a crucial role in directing product selectivity toward methanol or CO. Interestingly, at the highest temperature tested (340 °C), both CO_2 conversion (~50%) and methanol selectivity (~80%) converged for the 15, 30, and 50 wt % Cu−ZnO samples. These values align with thermodynamic expectations,[3,6] indicating that the reaction achieved thermodynamic equilibrium across all three catalysts at 340 °C. The 30 wt % Cu−ZnO catalyst stands out, achieving ~50% CO_2 conversion with 85% methanol selectivity, corresponding to a methanol weight time yield of 693 $mg_{(MeOH)}$ g_{cat}^{-1} h^{-1} at 280 °C, which is slightly lower than 885 $mg_{(MeOH)}$ g_{cat}^{-1} h^{-1} reported for commercial Cu-based catalysts under similar process conditions.[6]

To clarify their catalytic performance, Cu−ZnO materials were analyzed by XRD after reaction, as shown in Figure 10.

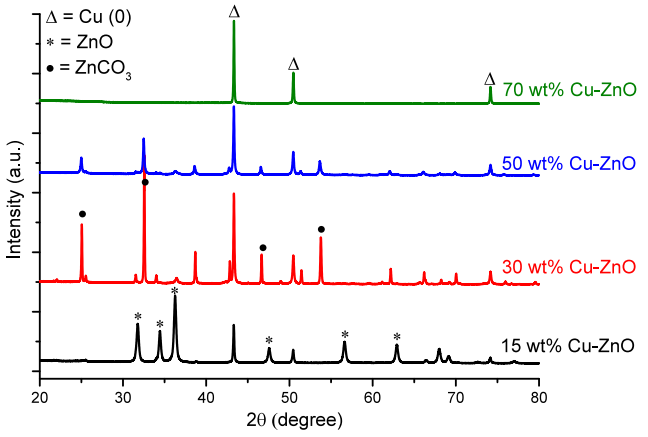

Figure 10. XRD of the catalysts after the reaction is presented in Figure 9.

The 70 wt % Cu−ZnO sample mainly exhibited Cu(0) reflections, while the 15 wt % Cu−ZnO sample primarily showed the ZnO phase with a minor presence of Cu(0). Intriguingly, $ZnCO_3$ was clearly formed in both 30 and 50 wt % Cu−ZnO samples, a result uncommon for methanol synthesis catalysts. Table 2 quantifies the crystal phases:

Table 2. Quantitative Phase Analysis of 30 and 50 wt % Cu−ZnO before and after the Reaction

	before reaction (wt %)		after reaction (wt %)	
component	30 wt %	50 wt %	30 wt %	50 wt %
Cu_2O	30.8	44.1	1.8	1.4
ZnO	69.2	55.9	0.4	1.3
Cu(0)			29.2	42.0
$ZnCO_3$			68.4	55.4

most Cu_2O was converted to Cu(0), as expected, while ZnO transformed into $ZnCO_3$. Assuming all Zn is crystalline and detectable by XRD, 98 and 99% of Zn exist as $ZnCO_3$ in the respective samples. This suggests that the presence of ZnO and its interaction with Cu may not be essential for high catalytic activity, at least as bulk materials; instead, the specific form of Cu likely plays a more critical role.

The top-performing material, 30 wt % Cu−ZnO, was examined post-reaction by the TEM and EDX line scan (Figures 11 and 12a). The initially partially filled Cu core became fully metallic with no shell deformation observed, though ZnO particles became sintered and more crystalline. Notably, copper particles did not agglomerate after 100 h at 331 bar across temperatures from 220 to 340 °C, demonstrating the excellent thermal stability of the Cu−ZnO structure.

STEM (Figure 12b) and EDX (Figure 12c−h) analyses revealed that the Zn shell transformed into $ZnCO_3$, supported by XRD data (Figure 10), with co-located Zn, O, and C distributions. Cu was also present in the shell region, showing a distribution different from that of Zn and overlaying the $ZnCO_3$ surface and cavities. This spread is consistent with both precursors being in solution during synthesis. The large Cu surface area after activation (10.6 m^2 g^{-1}) suggests that small Cu particles are present.

Assuming the presence of smooth, spherical Cu particles with diameters of 200, 500, and 1000 nm yields calculated surface areas of 3.3, 1.3, and 0.7 m^2 g^{-1}, respectively. These values indicate that highly dispersed copper particles are present within the material, likely contributing to the enhanced catalytic performance observed for the 30 wt % Cu−ZnO sample. In contrast, the Cu surface area for the low-activity 70 wt % Cu−ZnO sample was measured at 1.2 m^2 g^{-1}, closely corresponding to the surface area expected for particles around 500 nm in diameter. This suggests that the catalytic activity of the material primarily arises from the surface of the copper core, with notable methanol selectivity achieved at lower temperatures, i.e., a characteristic commonly attributed to larger crystallites featuring an extended copper surface.[15]

According to the literature, the formation of the $ZnCO_3$ (smithsonite) phase during methanol synthesis from CO/CO_2 has recently been reported. Ash-Kurlander et al. identified this phase in CO_2-based methanol synthesis, attributing its formation to acidic pH conditions that promote the dissolution of ZnO in aqueous carbonic acid and subsequent transformation to $ZnCO_3$.[79] Schulte et al. demonstrated reversible $ZnCO_3$ formation under high-pressure CO_2 hydrogenation but did not resolve clear relationships between catalyst morphology and methanol selectivity.[80] van Bokhoven et al. reported that methanol synthesis proceeds via a zinc formate intermediate pathway.[38] The effects of $ZnCO_3$ on the catalytic activity remain unclear. To investigate the relationship between $ZnCO_3$ formation and catalytic performance, the 30 wt % Cu−ZnO catalyst was evaluated under various pressure and temperature conditions (see Figure S3 of the Supporting Information) and characterized by XRD following the reaction (Figure S4 of the Supporting Information). The CO_2 conversion rate increased with a rising pressure. A shift in selectivity from CO to methanol at elevated pressures (331 bar), as previously discussed, appears related to both the reaction pressure and resultant catalytic activity (Figure S3 of the Supporting Information). XRD analysis (Figure S4 of the Supporting Information) revealed significant structural changes and clear formation of $ZnCO_3$ (JCPDS 00-008-0449) in samples tested at 331 bar compared to those evaluated at 27 and 184 bar. A further discussion regarding the origin of $ZnCO_3$ formation and its impact on catalytic performance will be discussed later.

3.6. Effects of Cu−Zn Proximity. The above study, which involved varying the Cu and Zn contents within a core−shell structure, demonstrated that the interaction between Cu and Zn is significant for catalytic activity. The results suggest the possible formation of a highly dispersed Cu particle or layer on

https://doi.org/10.1021/acs.energyfuels.5c03664
Energy Fuels 2025, 39, 22342−22355

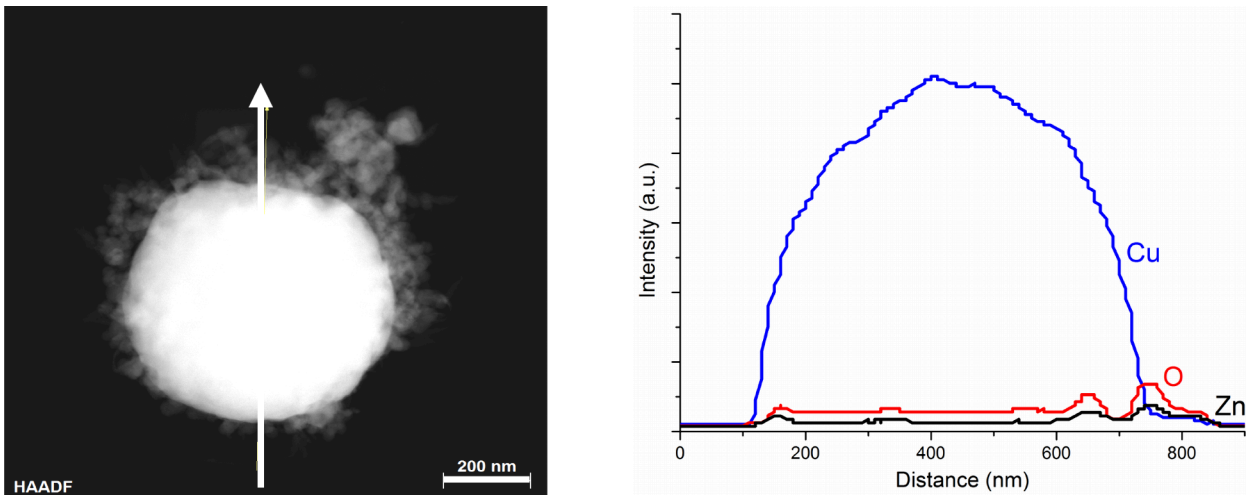

Figure 11. STEM and EDX line scan analysis of 30 wt % Cu−ZnO after the reaction.

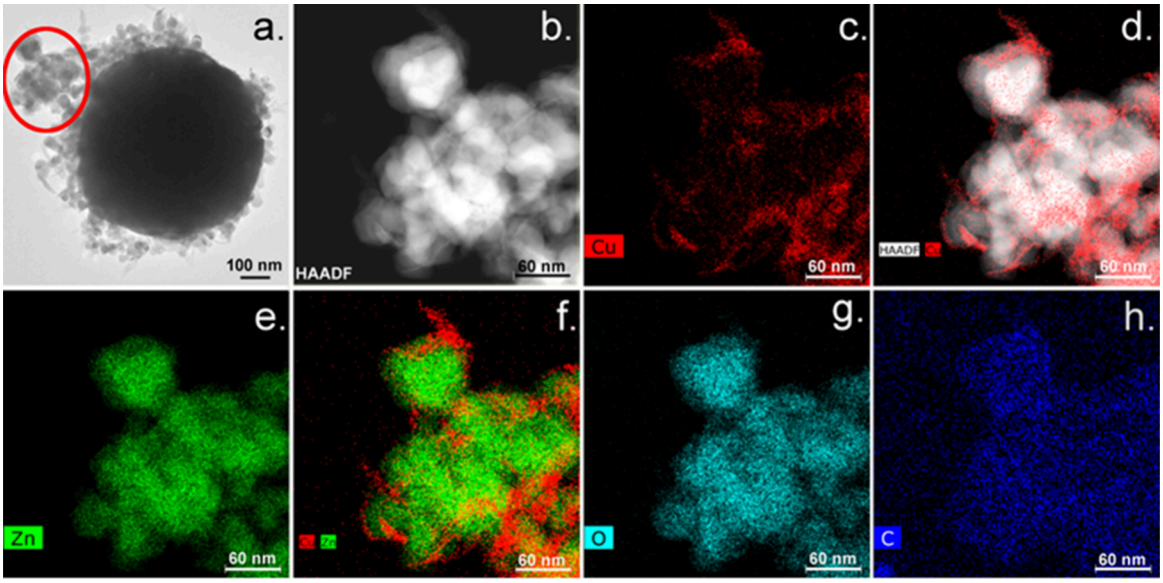

Figure 12. (a) TEM of 30 wt % Cu−ZnO after 100 h of reaction at 331 bar, 220−340 °C, and 4000 h^{-1} with prior catalyst reduction in H_2 at 330 °C and EDX analysis of the encircled region of the Zn shell: (b) STEM image, with elemental color mapping of (c) Cu, (d) overlay of the STEM image with Cu, (e) Zn, (f) overlay of Cu and Zn, (g) O, and (h) C.

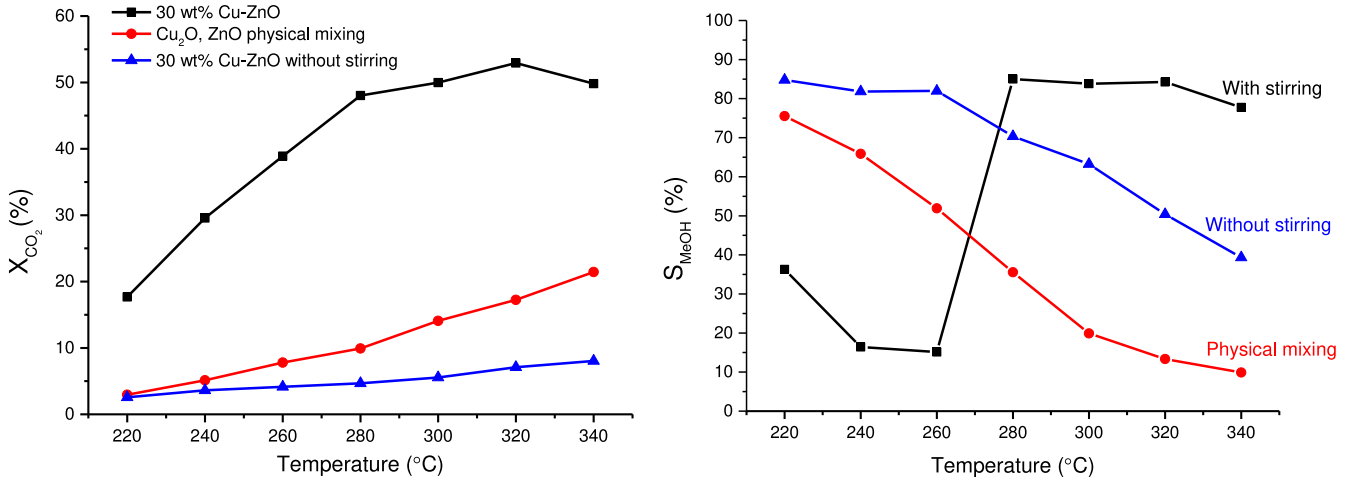

Figure 13. Comparison of CO_2 conversion (left) and methanol selectivity (right) of the (i) physical mixture of Cu_2O and ZnO and 30 wt % Cu−ZnO material synthesized (ii) with and (iii) without stirring under the standard reaction conditions (331 bar and 4000 h^{-1}).

https://doi.org/10.1021/acs.energyfuels.5c03664
Energy Fuels 2025, 39, 22342−22355

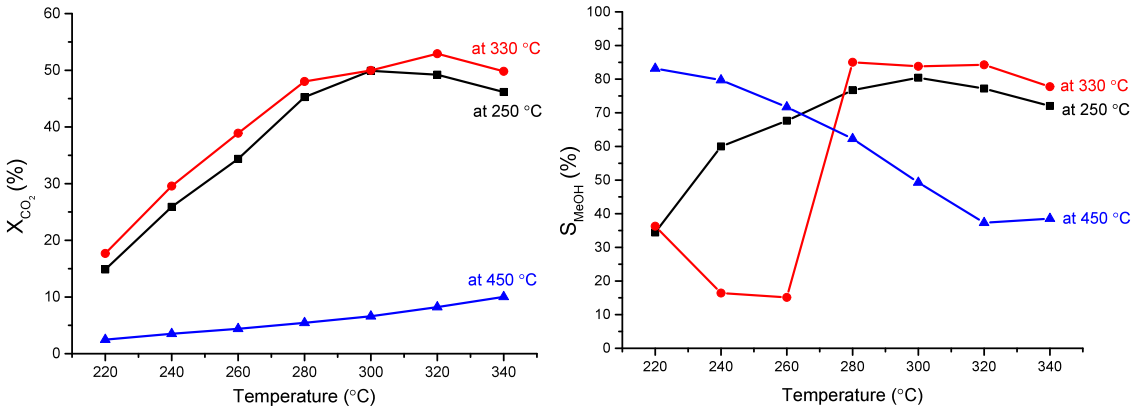

Figure 14. Effects of catalyst prereduction conditions of 30 wt % Cu_2O−ZnO on the catalytic performance under the standard reaction conditions (331 bar and 4000 h^{-1}).

the Zn-containing phase. To further investigate the synergistic role of Cu−ZnO, two materials with a fixed composition of 30 wt % Cu and 70 wt % ZnO were evaluated: (i) a physical mixture of Cu_2O and ZnO and (ii) Cu−ZnO synthesized without stirring (see Figure 1c). Their catalytic performances are presented in Figure 13.

Both the physical mixture of Cu_2O and ZnO as well as Cu−ZnO synthesized without stirring exhibited substantially lower catalytic activity compared to Cu−ZnO prepared with stirring. However, these two materials exhibited higher methanol selectivity at low CO_2 conversion (low temperature), indicating that direct methanol synthesis predominates under these conditions,[81] contrasting with the observations for the core−shell material. These findings underscore the importance of morphology and close contact between Cu and Zn components in achieving high-performance methanol synthesis, as such configurations provide Cu−Zn interfacial sites that are regarded as highly active phases, as demonstrated by atomic layer deposition.[42,45,82] Additionally, the results corroborate previous suggestions regarding elevated methanol selectivity at a low temperature for extended Cu surfaces, particularly in the context of 70 wt % Cu−ZnO systems.

3.7. Effects of the Pre-reduction Temperature. An important experimental parameter affecting the catalytic performance in methanol synthesis with Cu-based catalysts is the reduction pretreatment conducted under a H_2 atmosphere. Accordingly, this study evaluated the impact of the reduction temperature on the best performing material for methanol synthesis, specifically 30 wt % Cu_2O−ZnO, which was subjected to reduction at three distinct temperatures (250, 330, and 450 °C). These temperatures were selected to represent different catalyst states: prior to substantial reduction of the Cu_2O phase (250 °C), following major completion of Cu_2O reduction (330 °C), and after complete reduction of Cu_2O (450 °C), as determined by *in situ* XRD analysis (corresponding to red boxes in Figure 7).

The catalytic performance of Cu_2O−ZnO reduced at each temperature is depicted in Figure 14, highlighting the pronounced influence of pretreatment on activity. Catalysts reduced at 250 and 330 °C demonstrated comparable catalytic behavior, with several distinctions: (i) generally higher CO_2 conversion at 330 °C, (ii) greater methanol selectivity at lower temperatures (<270 °C) for the catalyst reduced at 250 °C, and (iii) enhanced methanol selectivity at elevated temperatures (>270 °C) when reduced at 330 °C. Although bulk reduction to metallic Cu was incomplete at 250 °C, it is likely that surface reduction occurred, supporting high catalytic activity.

Reduction at 450 °C led to a marked decline in catalytic performance, despite achieving the highest methanol selectivity below 270 °C (although direct comparison to other catalysts at similar CO_2 conversion was not performed). This decrease is primarily attributed to ZnO agglomeration and increased crystallinity, which reduce the dispersion of active Cu species and, thereby, limit CO_2 conversion. It should be noted that, while minor Cu surface sintering may occur at this temperature, the bulk Cu cores remain largely unsintered, indicating that the activity loss is dominated by changes in the ZnO phase rather than extensive Cu sintering. Post-reaction XRD analyses (Figure 15) revealed that the same material, when reduced at

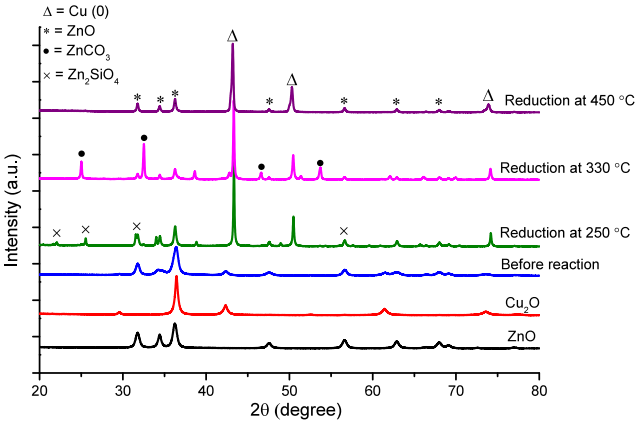

Figure 15. XRD of 30 wt % Cu_2O−ZnO reduced at 250, 330, and 450 °C and after the reaction under the standard conditions (331 bar, 220−340 °C, and 4000 h^{-1}). As a reference, the XRD patterns of the as-synthesized material, Cu_2O, and ZnO prepared by the non-aqueous sol−gel method are also shown.

different temperatures, exhibited significantly varied diffraction patterns. Notably, the material reduced to 330 °C predominantly formed $ZnCO_3$, as previously discussed.

To our surprise, this $ZnCO_3$ phase was not detected in the other two materials. When 30 wt % Cu_2O−ZnO was reduced at 250 °C, Zn_2SiO_4 (JCPDS 00-008-0492) was formed, despite the absence of an added silicon source in the reactor. In contrast, reduction at 450 °C did not result in new phase formation, with Zn present as ZnO. The higher temperature

https://doi.org/10.1021/acs.energyfuels.5c03664
Energy Fuels 2025, 39, 22342−22355

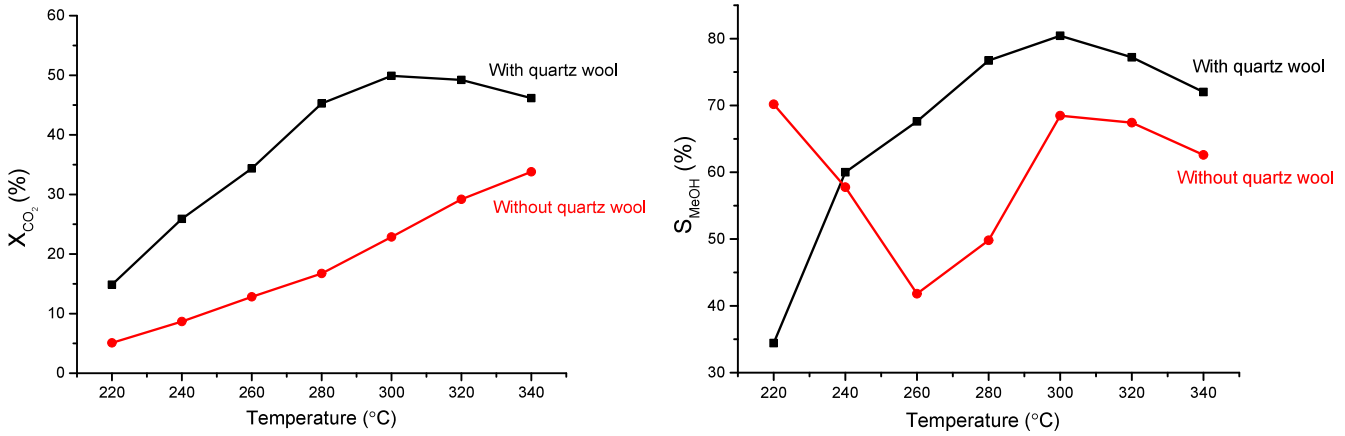

Figure 16. Catalytic performance of 30 wt % Cu_2O−ZnO reduced at 250 °C tested under the standard conditions with and without quartz wool to hold the catalyst in the reactor.

reduction produced stable ZnO, potentially accompanied by a loss of highly dispersed Cu under the reaction conditions. These results indicate that ZnO in the 30 wt % Cu_2O−ZnO material exhibits high reactivity, particularly upon low-temperature reduction, and adjusts its state according to environmental factors.

The occurrence of Zn_2SiO_4 has not been previously documented, which makes this finding notable. As described in the catalytic tests, quartz wool used to fix the catalyst bed is the only silicon source in the system, suggesting that highly active ZnO after low-temperature reduction can interact with quartz in contact with the material. To assess the impact of Zn_2SiO_4 formation on catalytic activity, reactions were conducted without quartz wool instead using a 10 μm stainless-steel frit to hold the catalyst.

Figure 16 presents a comparison of the catalytic performance with and without quartz wool. A higher catalytic performance was observed when quartz wool was used. In the absence of quartz wool, no Zn_2SiO_4 phase was observed after the reaction; only ZnO was detected (Figure S5 of the Supporting Information). While the precise role of Zn_2SiO_4 is not studied here, a similar catalytic performance for materials reduced at 250 and 330 °C suggests that the specific state of the Zn component may be less critical for catalytic performance than the effect of its state and morphology on Cu. The structural features of Zn_2SiO_4 and $ZnCO_3$ likely facilitate a greater dispersion of Cu sites (crystallite sizes: $ZnCO_3$, 72 nm; Zn_2SiO_4, 60 nm; see Figure 12). Conversely, although the Cu core does not undergo sintering after reduction at 450 °C, the catalytic activity decreases significantly. This is likely due to increased ZnO crystallinity, as ZnO agglomerates and grows from 20 to 229 nm, reducing the surface area and, thereby, decreasing the dispersion of active Cu species.

3.8. *Operando* XRD. To clarify the conditions for $ZnCO_3$ phase formation in Cu−ZnO catalysts, *operando* high-pressure XRD was conducted (see Figure S6 of the Supporting Information). Initial trials with 30 wt % Cu−ZnO were unsuccessful due to excessive pressure drop and poor catalytic performance from small particles (<10 μm); thus, no ZnO phase change was seen. Therefore, the structure of a commercial $Cu/ZnO/Al_2O_3$ methanol synthesis catalyst was studied before and after the reaction to assess if $ZnCO_3$ forms generally in Cu−ZnO-based catalysts.

Figure 17 shows first the *ex situ* XRD results at pressures of 92, 331, and 442 bar. The results indicate that $ZnCO_3$ formation commonly occurs in Cu−Zn catalytic systems, with an increased formation observed at elevated pressures. Analysis of the XRD patterns shows that the initial ZnO phase is progressively replaced by $ZnCO_3$ as the reaction pressure increases, along with higher crystallinity in both the Cu and Zn phases.

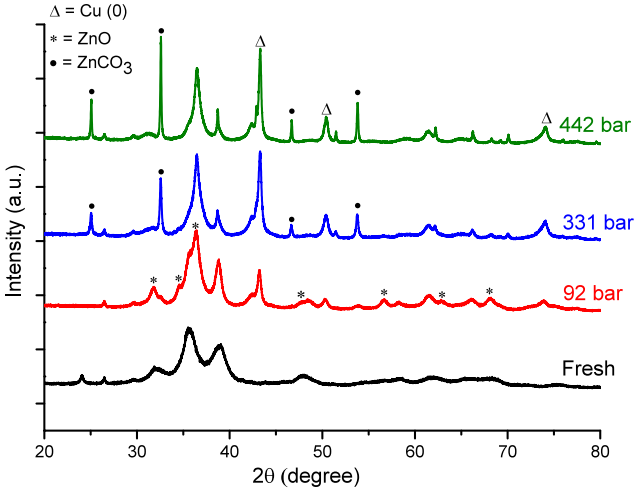

Figure 17. XRD patterns of the commercial $Cu/ZnO/Al_2O_3$ catalyst after reaction at different reaction pressures at 220−300 °C and 10 000 h^{-1} after catalyst reduction at 330 °C.

Figure 18 displays *operando* XRD patterns for the commercial $Cu/ZnO/Al_2O_3$ catalyst during stoichiometric CO_2 hydrogenation to methanol at 184 bar and a reaction temperature of 300 °C after reduction at 330 °C (see the Supporting Information for the experimental procedure). The study evidently demonstrates that $ZnCO_3$ forms rapidly and continuously under high-pressure reaction conditions rather than as a result of post-reaction exposure to air (the stabilized structure of $ZnCO_3$ under *operando* conditions at 331 bar after the reaction at 184 bar is shown in Figures S6 and S7).

3.9. Relation between $ZnCO_3$ Formation and Catalytic Activity. Figures S6 and S7 of the Supporting Information and Figure 17 provide evidence of $ZnCO_3$ formation under high-pressure conditions, while similar

https://doi.org/10.1021/acs.energyfuels.5c03664
Energy Fuels 2025, 39, 22342−22355

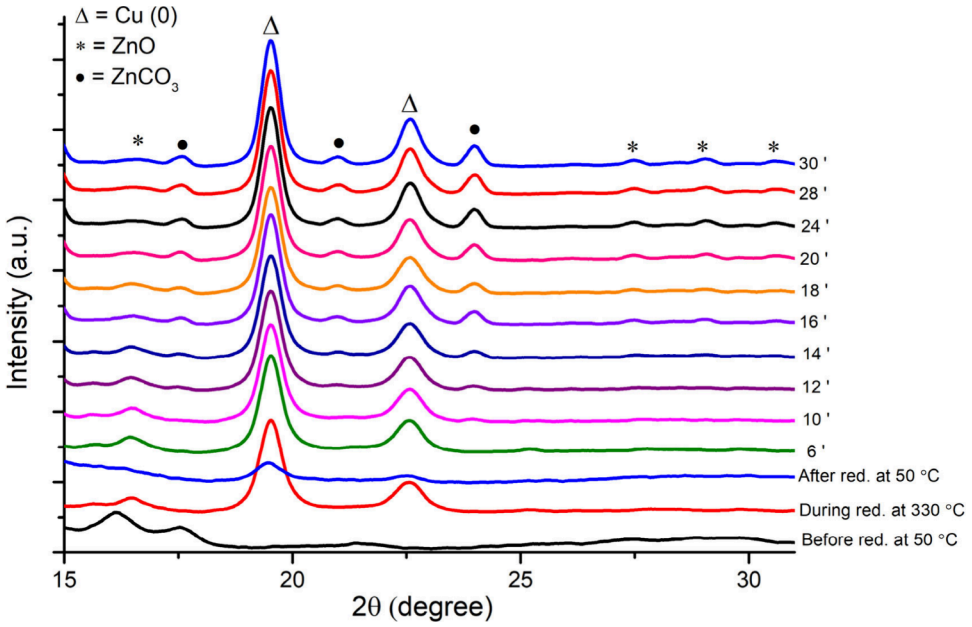

Figure 18. *Operando* XRD of the commercial $Cu/ZnO/Al_2O_3$ catalyst at CO_2/H_2 = 1:3, 184 bar, and 300 °C after reduction at 330 °C. The number on the right shows the reaction time in minutes (6′, 10′, ...) when the catalyst was exposed to the reaction mixture.

formation was also observed at a lower pressure for the commercial catalyst (e.g., 92 bar). This suggests that the formation may not be solely attributable to high-pressure conditions but could instead be associated with increased reactivity,[6] specifically related to the creation of a dense product phase (liquid/supercritical), which typically occurs under high-pressure conditions.

A notable selectivity change from CO to methanol occurred within a narrow temperature range of 260−280 °C as the reaction temperature increased for 30 wt % Cu−ZnO reduced at 330 °C (see Figure 9). To determine the material factors influencing product selectivity, samples after reactions at 260 and 280 °C were examined by XRD. Results shown in Figure 19 illustrate the differences in the XRD patterns, with clear evidence of $ZnCO_3$ formation at 280 °C. The proportions of Zn-containing phases ($ZnCO_3$/ZnO) were 0.0/69.2 wt % at 260 °C and 66.4/2.4 wt % at 280 °C, as determined by quantitative phase analysis. These observations support the interpretation that the phase transformation is more closely linked to product formation than to reaction pressure.

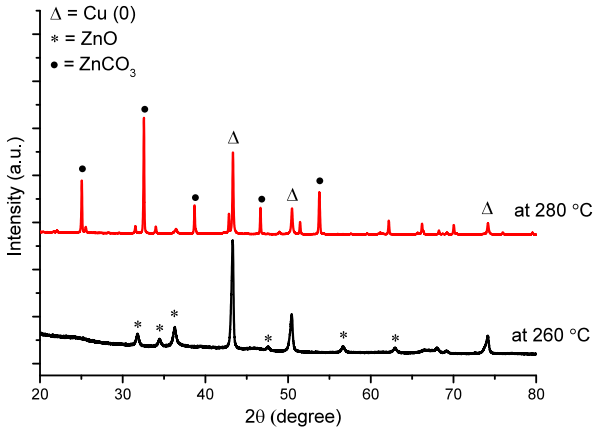

Figure 19. XRD patterns of the 30 wt % Cu−ZnO catalyst reduced at 330 °C after the reaction at 260 or 280 °C, 331 bar, and 4000 h^{-1}.

At temperatures above 280 °C, methanol selectivity was significantly enhanced for the 30 wt % Cu−ZnO catalyst (Figure 9). A key question remains: Is this highly dispersed state of Cu over $ZnCO_3$ (Figure 12) responsible for the increased methanol selectivity? To investigate this, catalytic reactions were conducted using ramp-up and ramp-down cycles repeated twice. The resulting catalytic performance is presented in Figure 20. Following the initial ramp-up, some catalyst deactivation was observed based on CO_2 conversion measurements; however, subsequent activity remained relatively stable, with only a slight continuous decrease in CO_2 conversion, potentially due to irreversible structural changes from exposure to elevated temperatures (up to 340 °C).

In contrast, methanol selectivity exhibited more pronounced fluctuations during each ramp-up and ramp-down step. In the first ramp-down, a decline in methanol selectivity was noted in the mid-temperature range, with the minimum selectivity temperature shifting higher. The second ramp-up produced a similar profile, albeit with slightly improved methanol selectivity. Notably, during the second cycle's ramp-down, the decrease in selectivity was less significant and became more stable.

The recurring drop in methanol selectivity in the mid-temperature range throughout the cycles suggests that these changes are not directly attributable to the interaction between Cu and $ZnCO_3$. Instead, they are likely governed by the catalyst's momentary activity and phase behavior, such as product condensation dictated by product quantity. During the initial ramp-up, the formation of water and high CO_2 pressure may promote the development of a highly acidic, liquid, or dense phase containing carbonic acid, leading to extensive transformation of ZnO into $ZnCO_3$, consistent with observations of pressure-dependent $ZnCO_3$ formation in commercial catalysts (Figure 17). The *operando* XRD study revealed that the formed $ZnCO_3$ phase is highly stable and remains irreversible under the process conditions. As shown in

https://doi.org/10.1021/acs.energyfuels.5c03664
Energy Fuels 2025, 39, 22342−22355

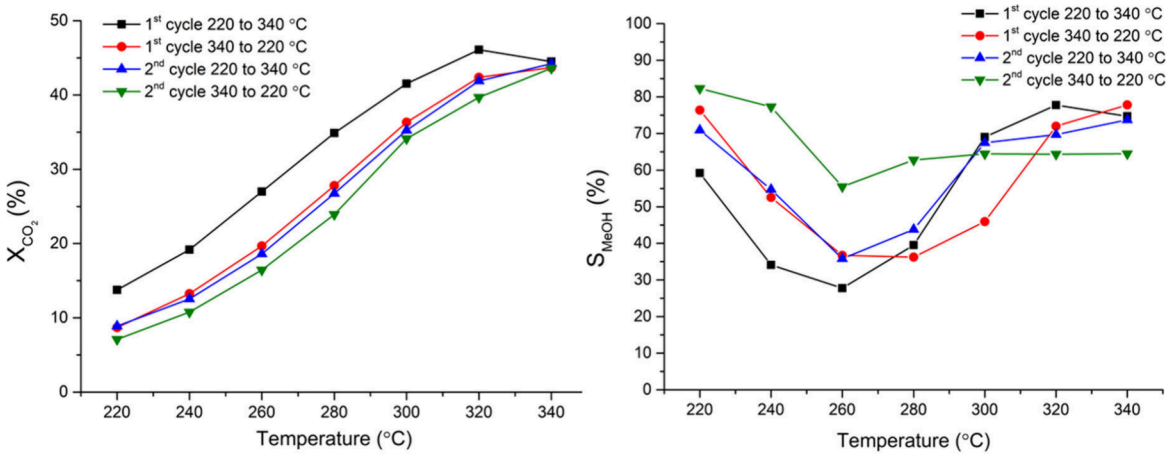

Figure 20. Effects of temperature ramp-up and ramp-down on the catalytic performance of 30 wt % Cu−ZnO at 331 bar, 220−340 °C, and 4000 h^{-1} and reduced in H_2 at 330 °C.

Figure S9, it decomposes only when the temperature is increased to 500 °C, leading to regeneration of the ZnO phase.

With successive cycles, a partial loss of catalytic activity likely results from further $ZnCO_3$ crystallization and concomitant Cu sintering. Importantly, this stabilized state appears to be advantageous for enhancing methanol selectivity at lower temperatures, accompanied by only a minor reduction in CO_2 conversion. These findings align with prior discussions and the reported high methanol selectivity on extended Cu surfaces during CO_2 hydrogenation. The resulting porous yet robust $ZnCO_3$ structure may offer marked benefits for both catalyst stability and methanol selectivity.

4. CONCLUSION

A surfactant-free, non-aqueous sol−gel approach was developed for the synthesis of Cu−ZnO core−shell materials, aiming to investigate the distinctive Cu−Zn interface relevant for methanol production and to improve the thermal stability of active Cu sites. By varying the proportions of Cu and Zn precursors, Cu_2O−ZnO core−shell architectures were successfully achieved, featuring Cu_2O cores enveloped by highly dispersed ZnO nanoparticle layers.

The catalyst comprising 30 wt % Cu_2O−ZnO exhibited superior performance, delivering 53% CO_2 conversion and 84% methanol selectivity during stoichiometric CO_2 hydrogenation to methanol at 331 bar. This enhanced catalytic activity was attributed primarily to the unique distribution of Cu within the shell rather than solely to the core−shell configuration. Under reaction conditions, the core−shell morphology remained intact; however, significant phase transformation of the ZnO shell to $ZnCO_3$ was observed. Electron microscopy revealed that Cu in the shell became finely dispersed across what is likely a rigid, porous $ZnCO_3$ nanomaterial matrix. The formation of $ZnCO_3$ correlated with increased methanol selectivity and showed a dependence on pressure, suggesting that this phase transition results from the highly acidic environment generated by CO_2 and H_2O under elevated pressures, only manifesting above certain thresholds of reaction pressure and CO_2 conversion. High-pressure *operando* XRD studies with commercial Cu/ZnO/Al_2O_3 catalysts confirmed the general occurrence of $ZnCO_3$ formation under such conditions.

Investigations into the effects of Cu−ZnO proximity and pre-reduction temperature indicated that nanoscale contact between Cu and ZnO significantly influences catalytic activity. While high methanol selectivity at low temperatures was consistently observed in samples where Cu was agglomerated, typically with reduced Cu−ZnO contact or elevated reduction temperatures, these materials demonstrated lower CO_2 conversion rates. The reduction temperature notably affected the reactivity of the ZnO shell: following reaction at 331 bar, $ZnCO_3$ and Zn_2SiO_4 phases formed in samples reduced at 330 and 250 °C, respectively, whereas only ZnO was present when reduced at 450 °C. These disparities underscore the impact of reduction conditions, yet the specific Zn phase appears less critical for catalytic performance compared to the dispersion state of Cu; the sintering behavior of the Zn component is a more decisive factor.

The findings indicate that the Cu core and ZnO shell structures are advantageous for maintaining Cu dispersion at the core dimension. However, the principal catalytic activity stems from Cu nanoparticles or layers intimately associated with the Zn-containing matrix within the shell. The non-aqueous sol−gel method proved highly effective and adaptable for designing Cu−ZnO-based nanomaterials. Future research leveraging this synthesis technique may focus on optimizing Cu dispersion in straightforward Cu−ZnO nanocomposites or minimizing the Cu core size to further enhance the activity and stability of Cu−ZnO catalysts.

■ ASSOCIATED CONTENT

Supporting Information

The Supporting Information is available free of charge at https://pubs.acs.org/doi/10.1021/acs.energyfuels.5c03664.

Experimental details of *ex situ*, *in situ*, and *operando* XRD, Cu surface area and crystallite size of the Cu_2O−ZnO core−shell materials, summary of the TPR results, pressure effects on the catalytic performance and catalyst structure (XRD patterns) of 30 wt % Cu_2O−ZnO, XRD of the 30 wt % Cu_2O−ZnO catalyst after reduction at 250 °C and reaction with and without quartz wool, *operando* XRD of the Cu/ZnO/Al_2O_3 catalysts at CO_2/H_2 = 1:3, 331 bar, and 200 °C of the used catalyst after reaction at 184 bar at 300 °C, *operando* XRD of the Cu/ZnO/Al_2O_3 catalysts at CO_2/H_2 = 1:3, 331 bar, and 300 °C of the used catalyst after reaction at 331 bar at 220

https://doi.org/10.1021/acs.energyfuels.5c03664
Energy Fuels 2025, 39, 22342−22355

°C, and SEM images of Cu_2O particles and 30 wt % Cu_2O−ZnO prepared with stirring (PDF)

AUTHOR INFORMATION

Corresponding Author

Atsushi Urakawa − *Institute of Chemical Research of Catalonia (ICIQ), The Barcelona Institute of Science and Technology, 43007 Tarragona, Spain; Catalysis Engineering, Department of Chemical Engineering, Delft University of Technology, 2629 HZ Delft, Netherlands;* orcid.org/0000-0001-7778-4008; Email: a.urakawa@tudelft.nl

Authors

Rohit Gaikwad − *Institute of Chemical Research of Catalonia (ICIQ), The Barcelona Institute of Science and Technology, 43007 Tarragona, Spain;* Present Address: Elplatek A/S, Meteorvej 10, 8700 Horsens, Denmark

Niklaus Kränzlin − *Laboratory for Multifunctional Materials, Department of Materials, ETH Zurich, 8093 Zurich, Switzerland*

Jordi Benet-Buchholz − *Institute of Chemical Research of Catalonia (ICIQ), The Barcelona Institute of Science and Technology, 43007 Tarragona, Spain;* orcid.org/0000-0003-3984-3550

Markus Niederberger − *Laboratory for Multifunctional Materials, Department of Materials, ETH Zurich, 8093 Zurich, Switzerland;* orcid.org/0000-0001-6058-1183

Dorota Koziej − *Laboratory for Multifunctional Materials, Department of Materials, ETH Zurich, 8093 Zurich, Switzerland; Institute for Nanostructure and Solid-State Physics, Center for Hybrid Nanostructures, University of Hamburg, Hamburg 22761, Germany;* orcid.org/0000-0002-9064-2642

Complete contact information is available at: https://pubs.acs.org/10.1021/acs.energyfuels.5c03664

Author Contributions

The manuscript was written through contributions of all authors. All authors have given approval to the final version of the manuscript.

Notes

The authors declare no competing financial interest.

ACKNOWLEDGMENTS

The authors thank the financial support from the ICIQ Foundation and MINECO (CTQ2012-34153). R.G. acknowledges MINECO for the FPI Predoctoral Fellowship (EEBB-I-15-10528).

REFERENCES

(1) Olah, G. A.; Goeppert, A.; Prakash, G. K. S. The "Methanol Economy": General Aspects. *Beyond Oil and Gas: The Methanol Economy*; Wiley-VCH Verlag GmbH & Co. KGaA: Weinheim, Germany, 2009; Chapter 10, pp 179−184, DOI: 10.1002/9783527627806.ch10.

(2) Centi, G.; Perathoner, S. Opportunities and prospects in the chemical recycling of carbon dioxide to fuels. *Catal. Today* **2009**, *148* (3−4), 191−205.

(3) Álvarez, A.; Bansode, A.; Urakawa, A.; Bavykina, A. V.; Wezendonk, T. A.; Makkee, M.; Gascon, J.; Kapteijn, F. Challenges in the Greener Production of Formates/Formic Acid, Methanol, and DME by Heterogeneously Catalyzed CO_2 Hydrogenation Processes. *Chem. Rev.* **2017**, *117* (14), 9804−9838.

(4) Jiang, X.; Nie, X. W.; Guo, X. W.; Song, C. S.; Chen, J. G. G. Recent Advances in Carbon Dioxide Hydrogenation to Methanol via Heterogeneous Catalysis. *Chem. Rev.* **2020**, *120* (15), 7984−8034.

(5) Bansode, A.; Urakawa, A. Towards full one-pass conversion of carbon dioxide to methanol and methanol-derived products. *J. Catal.* **2014**, *309*, 66−70.

(6) Gaikwad, R.; Bansode, A.; Urakawa, A. High-pressure advantages in stoichiometric hydrogenation of carbon dioxide to methanol. *J. Catal.* **2016**, *343*, 127−132.

(7) Phongprueksathat, N.; Ting, K. W.; Mine, S.; Jing, Y.; Toyoshima, R.; Kondoh, H.; Shimizu, K.; Toyao, T.; Urakawa, A. Bifunctionality of Re Supported on TiO_2 in Driving Methanol Formation in Low-Temperature CO_2 Hydrogenation. *ACS Catal.* **2023**, *13* (16), 10734−10750.

(8) Carmo, M.; Fritz, D. L.; Mergel, J.; Stolten, D. A comprehensive review on PEM water electrolysis. *Int. J. Hydrogen Energy* **2013**, *38* (12), 4901−4934.

(9) Zeng, K.; Zhang, D. K. Recent progress in alkaline water electrolysis for hydrogen production and applications. *Prog. Energy Combust. Sci.* **2010**, *36* (3), 307−326.

(10) Nikolaidis, P.; Poullikkas, A. A comparative overview of hydrogen production processes. *Renewable & Sustainable Energy Reviews* **2017**, *67*, 597−611.

(11) Zhu, J.; Hu, L. S.; Zhao, P. X.; Lee, L. Y. S.; Wong, K. Y. Recent Advances in Electrocatalytic Hydrogen Evolution Using Nanoparticles. *Chem. Rev.* **2020**, *120* (2), 851−918.

(12) Wang, W.; Wang, S.; Ma, X.; Gong, J. Recent advances in catalytic hydrogenation of carbon dioxide. *Chem. Soc. Rev.* **2011**, *40* (7), 3703−3727.

(13) Martin, O.; Mondelli, C.; Cervellino, A.; Ferri, D.; Curulla-Ferre, D.; Perez-Ramirez, J. Operando Synchrotron X-ray Powder Diffraction and Modulated-Excitation Infrared Spectroscopy Elucidate the CO_2 Promotion on a Commercial Methanol Synthesis Catalyst. *Angew. Chem.* **2016**, *55*, 11031.

(14) Huang, C.; Chen, S.; Fei, X.; Liu, D.; Zhang, Y. Catalytic Hydrogenation of CO_2 to Methanol: Study of Synergistic Effect on Adsorption Properties of CO_2 and H_2 in CuO/ZnO/ZrO_2 System. *Catalysts* **2015**, *5* (4), 1846−1861.

(15) Bansode, A.; Tidona, B.; von Rohr, P. R.; Urakawa, A. Impact of K and Ba promoters on CO_2 hydrogenation over Cu/Al_2O_3 catalysts at high pressure. *Catal. Sci. Technol.* **2013**, *3* (3), 767−778.

(16) Phongprueksathat, N.; Bansode, A.; Toyao, T.; Urakawa, A. Greener and facile synthesis of Cu/ZnO catalysts for CO_2 hydrogenation to methanol by urea hydrolysis of acetates. *Rsc Advances* **2021**, *11* (24), 14323−14333.

(17) Meunier, F. C. Mixing Copper Nanoparticles and ZnO Nanocrystals: A Route towards Understanding the Hydrogenation of CO_2 to Methanol? *Angew. Chem., Int. Ed.* **2011**, *50* (18), 4053−4054.

(18) Spencer, M. S. The role of zinc oxide in Cu/ZnO catalysts for methanol synthesis and the water−gas shift reaction. *Top. Catal.* **1999**, *8* (3), 259−266.

(19) Wambach, J.; Baiker, A.; Wokaun, A. CO_2 hydrogenation over metal/zirconia catalysts. *Phys. Chem. Chem. Phys.* **1999**, *1* (22), 5071−5080.

(20) Kuld, S.; Conradsen, C.; Moses, P. G.; Chorkendorff, I.; Sehested, J. Quantification of zinc atoms in a surface alloy on copper in an industrial-type methanol synthesis catalyst. *Angew. Chem.* **2014**, *53* (23), 5941−5945.

(21) Beck, A.; Newton, M. A.; van de Water, L. G. A.; van Bokhoven, J. A. The Enigma of Methanol Synthesis by Cu/ZnO/Al_2O_3-Based Catalysts. *Chem. Rev.* **2024**, *124* (8), 4543−4678.

(22) Larmier, K.; Liao, W. C.; Tada, S.; Lam, E.; Verel, R.; Bansode, A.; Urakawa, A.; Comas-Vives, A.; Copéret, C. CO_2-to-Methanol Hydrogenation on Zirconia-Supported Copper Nanoparticles: Reaction Intermediates and the Role of the Metal-Support Interface. *Angew. Chem., Int. Ed.* **2017**, *56* (9), 2318−2323.

(23) Szanyi, J.; Goodman, D. W. Methanol synthesis on a Cu(100) catalyst. *Catal. Lett.* **1991**, *10* (5), 383−390.

(24) Klier, K.; Chatikavanij, V.; Herman, R. G.; Simmons, G. W. Catalytic synthesis of methanol from COH_2. *J. Catal.* **1982**, *74* (2), 343−360.
(25) Tang, Q.-L.; Zou, W.-T.; Huang, R.-K.; Wang, Q.; Duan, X.-X. Effect of the components' interface on the synthesis of methanol over Cu/ZnO from CO_2/H_2: a microkinetic analysis based on DFT + *U* calculations. *Phys. Chem. Chem. Phys.* **2015**, *17* (11), 7317−7333.
(26) Zander, S.; Kunkes, E. L.; Schuster, M. E.; Schumann, J.; Weinberg, G.; Teschner, D.; Jacobsen, N.; Schlogl, R.; Behrens, M. The role of the oxide component in the development of copper composite catalysts for methanol synthesis. *Angew. Chem.* **2013**, *52* (25), 6536−6540.
(27) Karelovic, A.; Bargibant, A.; Fernández, C.; Ruiz, P. Effect of the structural and morphological properties of Cu/ZnO catalysts prepared by citrate method on their activity toward methanol synthesis from CO_2 and H_2 under mild reaction conditions. *Catal. Today* **2012**, *197* (1), 109−118.
(28) Zhang, L.; Zhang, Y.; Chen, S. Effect of promoter SiO_2, TiO_2 or SiO_2−TiO_2 on the performance of CuO−ZnO−Al_2O_3 catalyst for methanol synthesis from CO_2 hydrogenation. *Applied Catalysis A: General* **2012**, *415*−*416*, 118−123.
(29) Kuhl, S.; Tarasov, A.; Zander, S.; Kasatkin, I.; Behrens, M. Cu-based catalyst resulting from a Cu,Zn,Al hydrotalcite-like compound: a microstructural, thermoanalytical, and in situ XAS study. *Chemistry* **2014**, *20* (13), 3782−3792.
(30) Martinez-Suarez, L.; Frenzel, J.; Marx, D.; Meyer, B. Tuning the reactivity of a Cu/ZnO nanocatalyst via gas phase pressure. *Physical review letters* **2013**, *110* (8), No. 086108.
(31) Graciani, J.; Mudiyanselage, K.; Xu, F.; Baber, A. E.; Evans, J.; Senanayake, S. D.; Stacchiola, D. J.; Liu, P.; Hrbek, J.; Sanz, J. F.; et al. Highly active copper-ceria and copper-ceria-titania catalysts for methanol synthesis from CO_2. *Science* **2014**, *345* (6196), 546−550.
(32) Behrens, M.; Studt, F.; Kasatkin, I.; Kühl, S.; Hävecker, M.; Abild-Pedersen, F.; Zander, S.; Girgsdies, F.; Kurr, P.; Kniep, B.-L.; et al. The Active Site of Methanol Synthesis over Cu/ZnO/Al_2O_3 Industrial Catalysts. *Science* **2012**, *336* (6083), 893−897.
(33) Yang, Y.; Evans, J.; Rodriguez, J. A.; White, M. G.; Liu, P. Fundamental studies of methanol synthesis from CO(2) hydrogenation on Cu(111), Cu clusters, and Cu/ZnO(0001). *Physical chemistry chemical physics: PCCP* **2010**, *12* (33), 9909−9917.
(34) Studt, F.; Behrens, M.; Kunkes, E. L.; Thomas, N.; Zander, S.; Tarasov, A.; Schumann, J.; Frei, E.; Varley, J. B.; Abild-Pedersen, F.; et al. The Mechanism of CO and CO_2 Hydrogenation to Methanol over Cu-Based Catalysts. *ChemCatChem.* **2015**, *7* (7), 1105−1111.
(35) Studt, F.; Abild-Pedersen, F.; Varley, J. B.; Nørskov, J. K. CO and CO_2 Hydrogenation to Methanol Calculated Using the BEEF-vdW Functional. *Catal. Lett.* **2013**, *143* (1), 71−73.
(36) Wang, Z.-Q.; Xu, Z.-N.; Peng, S.-Y.; Zhang, M.-J.; Lu, G.; Chen, Q.-S.; Chen, Y.; Guo, G.-C. High-Performance and Long-Lived Cu/SiO_2 Nanocatalyst for CO_2 Hydrogenation. *ACS Catal.* **2015**, *5* (7), 4255−4259.
(37) Pandit, L.; Boubnov, A.; Behrendt, G.; Mockenhaupt, B.; Chowdhury, C.; Jelic, J.; Hansen, A. L.; Saraçi, E.; Ras, E. J.; Behrens, M.; et al. Unravelling the Zn−Cu Interaction during Activation of a Zn-promoted Cu/MgO Model Methanol Catalyst. *ChemCatChem.* **2021**, *13* (19), 4120−4132.
(38) Zabilskiy, M.; Sushkevich, V. L.; Palagin, D.; Newton, M. A.; Krumeich, F.; van Bokhoven, J. A. The unique interplay between copper and zinc during catalytic carbon dioxide hydrogenation to methanol. *Nat. Commun.* **2020**, *11* (1), 2409.
(39) Prieto, G.; Zečević, J.; Friedrich, H.; de Jong, K. P.; de Jongh, P. E. Towards stable catalysts by controlling collective properties of supported metal nanoparticles. *Nat. Mater.* **2013**, *12* (1), 34−39.
(40) Natesakhawat, S.; Lekse, J. W.; Baltrus, J. P.; Ohodnicki, P. R.; Howard, B. H.; Deng, X.; Matranga, C. Active Sites and Structure−Activity Relationships of Copper-Based Catalysts for Carbon Dioxide Hydrogenation to Methanol. *ACS Catal.* **2012**, *2* (8), 1667−1676.
(41) Grunwaldt, J.-D.; Molenbroek, A. M.; Topsøe, N.-Y.; Topsøe, H.; Clausen, B. S. In situ investigations of structural changes in Cu/ZnO catalysts. *J. Catal.* **2000**, *194* (2), 452−460.
(42) Tisseraud, C.; Comminges, C.; Belin, T.; Ahouari, H.; Soualah, A.; Pouilloux, Y.; Le Valant, A. The Cu−ZnO synergy in methanol synthesis from CO_2, Part 2: Origin of the methanol and CO selectivities explained by experimental studies and a sphere contact quantification model in randomly packed binary mixtures on Cu−ZnO coprecipitate catalysts. *J. Catal.* **2015**, *330*, 533−544.
(43) Tisseraud, C.; Comminges, C.; Pronier, S.; Pouilloux, Y.; Le Valant, A. The Cu−ZnO synergy in methanol synthesis Part 3: Impact of the composition of a selective Cu@ZnO_x core−shell catalyst on methanol rate explained by experimental studies and a concentric spheres model. *J. Catal.* **2016**, *343*, 106.
(44) Kanai, Y.; Watanabe, T.; Fujitani, T.; Uchijima, T.; Nakamura, J. The synergy between Cu and ZnO in methanol synthesis catalysts. *Catal. Lett.* **1996**, *38* (3), 157−163.
(45) Zhou, H.; Docherty, S. R.; Phongprueksathat, N.; Chen, Z. X.; Bukhtiyarov, A. V.; Prosvirin, I. P.; Safonova, O. V.; Urakawa, A.; Copéret, C.; Müller, C. R.; et al. Combining Atomic Layer Deposition with Surface Organometallic Chemistry to Enhance Atomic-Scale Interactions and Improve the Activity and Selectivity of Cu−Zn/SiO_2 Catalysts for the Hydrogenation of CO_2 to Methanol. *Jacs Au* **2023**, *3*, 2536.
(46) Etim, U. J.; Song, Y. B.; Zhong, Z. Y. Improving the Cu/ZnO-Based Catalysts for Carbon Dioxide Hydrogenation to Methanol, and the Use of Methanol As a Renewable Energy Storage Media. *Frontiers in Energy Research* **2020**, *8*, 545431.
(47) García-Trenco, A.; White, E.; Shaffer, M.; Williams, C. A one-step Cu/ZnO quasi-homogeneous catalyst for DME production from syn-gas. *Catalysis Science & Technology* **2016**, *6* (12), 4389−4397.
(48) Saedy, S.; Newton, M.; Zabilskiy, M.; Lee, J.; Krumeich, F.; Ranocchiari, M.; van Bokhoven, J. Copper-zinc oxide interface as a methanol-selective structure in Cu−ZnO catalyst during catalytic hydrogenation of carbon dioxide to methanol. *Catalysis Science & Technology* **2022**, *12* (8), 2703−2716.
(49) Beck, A.; Zabilskiy, M.; Newton, M. A.; Safonova, O.; Willinger, M. G.; van Bokhoven, J. A. Following the structure of copper-zinc-alumina across the pressure gap in carbon dioxide hydrogenation. *Nature Catalysis* **2021**, *4* (6), 488−497.
(50) Urakawa, A. Mind the gaps in CO_2-to-methanol. *Nature Catalysis* **2021**, *4* (6), 447−448.
(51) Rusdan, N. A.; Timmiati, S. N.; Isahak, W.; Yaakob, Z.; Lim, K. L.; Khaidar, D. Recent Application of Core−Shell Nanostructured Catalysts for CO_2 Thermocatalytic Conversion Processes. *Nanomaterials* **2022**, *12* (21), 3877.
(52) Kurtz, M.; Strunk, J.; Hinrichsen, O.; Muhler, M.; Fink, K.; Meyer, B.; Woll, C. Active sites on oxide surfaces: ZnO-catalyzed synthesis of methanol from CO and H_2. *Angew. Chem.* **2005**, *44* (18), 2790−2794.
(53) Kiennemann, A.; Idriss, H.; Hindermann, J. P.; Lavalley, J. C.; Vallet, A.; Chaumette, P.; Courty, P. Methanol synthesis on Cu/$ZnAl_2O_4$ and Cu/ZnOAl_2O_3 Catalysts. *Applied Catalysis* **1990**, *59* (1), 165−184.
(54) Millar, G. J.; Rochester, C. H.; Bailey, S.; Waugh, K. C. Combined temperature-programmed desorption and fourier-transform infrared spectroscopy study of CO_2, CO and H_2 interactions with model ZnO/SiO_2, Cu/SiO_2 and Cu/ZnO/SiO_2 methanol synthesis catalysts. *Journal of the Chemical Society, Faraday Transactions* **1993**, *89* (7), 1109−1115.
(55) Jadhav, S. G.; Vaidya, P. D.; Bhanage, B. M.; Joshi, J. B. Catalytic carbon dioxide hydrogenation to methanol: A review of recent studies. *Chem. Eng. Res. Des.* **2014**, *92* (11), 2557−2567.
(56) Ahouari, H.; Soualah, A.; Le Valant, A.; Pinard, L.; Magnoux, P.; Pouilloux, Y. Methanol synthesis from CO_2 hydrogenation over copper based catalysts. *Reaction Kinetics, Mechanisms and Catalysis* **2013**, *110* (1), 131−145.
(57) Lim, H.-W.; Park, M.-J.; Kang, S.-H.; Chae, H.-J.; Bae, J. W.; Jun, K.-W. Modeling of the Kinetics for Methanol Synthesis using

Cu/ZnO/Al_2O_3/ZrO_2 Catalyst: Influence of Carbon Dioxide during Hydrogenation. *Ind. Eng. Chem. Res.* **2009**, *48* (23), 10448−10455.
(58) Saito, M.; Takeuchi, M.; Watanabe, T.; Toyir, J.; Luo, S.; Wu, J. Methanol synthesis from CO_2 and H_2 over a CuZnO-based multicomponent catalyst. *Energy Conversion and Management* **1997**, *38*, S403−S408.
(59) Schumann, J.; Eichelbaum, M.; Lunkenbein, T.; Thomas, N.; Álvarez Galván, M. C.; Schlögl, R.; Behrens, M. Promoting Strong Metal Support Interaction: Doping ZnO for Enhanced Activity of Cu/ZnO:M (M = Al, Ga, Mg) Catalysts. *ACS Catal.* **2015**, *5* (6), 3260−3270.
(60) Li, J.; Guo, Q.; Zhao, X.; Hu, Y. K.; Zhang, S. Z.; Zhao, Y.; Li, S. Z. Effect of hydrothermal environment on Cu−ZnO/Al_2O_3 catalyst for hydrogenation of CO_2 to methanol. *Molecular Catalysis* **2023**, *549*, 113494.
(61) Liang, B. L.; Ma, J. G.; Su, X.; Yang, C. Y.; Duan, H. M.; Zhou, H. W.; Deng, S. L.; Li, L.; Huang, Y. Q. Investigation on Deactivation of Cu/ZnO/Al_2O_3 Catalyst for CO_2 Hydrogenation to Methanol. *Ind. Eng. Chem. Res.* **2019**, *58* (21), 9030−9037.
(62) *Methanol Production and Use*; Cheng, W.-H., Kung, H. H., Eds.; Marcel Dekker: New York, 1994.
(63) Nielsen, N.; Jensen, A.; Christensen, J. The roles of CO and CO_2 in high pressure methanol synthesis over Cu-based catalysts. *J. Catal.* **2021**, *393*, 324−334.
(64) Thrane, J.; Kuld, S.; Nielsen, N. D.; Jensen, A. D.; Sehested, J.; Christensen, J. M. Methanol-Assisted Autocatalysis in Catalytic Methanol Synthesis. *Angew. Chem., Int. Ed.* **2020**, *59* (41), 18189−18193.
(65) Wang, Z.; Fu, H.; Tian, Z.; Han, D.; Gu, F. Strong metal-support interaction in novel core−shell Au−CeO_2 nanostructures induced by different pretreatment atmospheres and its influence on CO oxidation. *Nanoscale* **2016**, *8* (11), 5865−5872.
(66) Kordus, D.; Widrinna, S.; Timoshenko, J.; Luna, M. L.; Rettenmaier, C.; Chee, S. W.; Ortega, E.; Karslioglu, O.; Kühl, S.; Cuenya, B. R. Enhanced Methanol Synthesis from CO_2 Hydrogenation Achieved by Tuning the Cu−ZnO Interaction in ZnO/Cu_2O Nanocube Catalysts Supported on ZrO_2 and SiO_2. *J. Am. Chem. Soc.* **2024**, *146* (12), 8677−8687.
(67) Guo, R. T.; Wang, J.; Bi, Z. X.; Chen, X.; Hu, X.; Pan, W. G. Recent Advances and Perspectives of Core−Shell Nanostructured Materials for Photocatalytic CO_2 Reduction. *Small* **2023**, *19* (9), 2206314.
(68) Jiang, R. Y.; Tung, S. O.; Tang, Z.; Li, L.; Ding, L.; Xi, X. G.; Liu, Y. Y.; Zhang, L.; Zhang, J. J. A review of core−shell nanostructured electrocatalysts for oxygen reduction reaction. *Energy Storage Materials* **2018**, *12*, 260−276.
(69) Li, L. M.; Su, J. Q.; Lu, J. M.; Shao, Q. Recent Advances of Core−Shell Cu-Based Catalysts for the Reduction of CO_2 to C_{2+} Products. *Chemistry - Asian Journal* **2023**, *18* (5), e202201044.
(70) Cushing, B. L.; Kolesnichenko, V. L.; O'Connor, C. J. Recent Advances in the Liquid-Phase Syntheses of Inorganic Nanoparticles. *Chem. Rev.* **2004**, *104* (9), 3893−3946.
(71) Niederberger, M. Nonaqueous Sol−Gel Routes to Metal Oxide Nanoparticles. *Acc. Chem. Res.* **2007**, *40* (9), 793−800.
(72) Niederberger, M.; Bartl, M. H.; Stucky, G. D. Benzyl Alcohol and Transition Metal Chlorides as a Versatile Reaction System for the Nonaqueous and Low-Temperature Synthesis of Crystalline Nano-Objects with Controlled Dimensionality. *J. Am. Chem. Soc.* **2002**, *124* (46), 13642−13643.
(73) Niederberger, M.; Garnweitner, G. Organic reaction pathways in the nonaqueous synthesis of metal oxide nanoparticles. *Chemistry* **2006**, *12* (28), 7282−7302.
(74) Garnweitner, G.; Niederberger, M. Nonaqueous and Surfactant-Free Synthesis Routes to Metal Oxide Nanoparticles. *J. Am. Ceram. Soc.* **2006**, *89* (6), 1801−1808.
(75) Pinna, N.; Garnweitner, G.; Antonietti, M.; Niederberger, M. Non-Aqueous Synthesis of High-Purity Metal Oxide Nanopowders Using an Ether Elimination Process. *Adv. Mater.* **2004**, *16* (23−24), 2196−2200.
(76) Evans, J. W.; Wainwright, M. S.; Bridgewater, A. J.; Young, D. J. On the determination of copper surface area by reaction with nitrous oxide. *Applied Catalysis* **1983**, *7* (1), 75−83.
(77) Kung, H. H. Deactivation of methanol synthesis catalysts—A review. *Catal. Today* **1992**, *11* (4), 443−453.
(78) Fierro, G.; Lojacono, M.; Inversi, M.; Porta, P.; Lavecchia, R.; Cioci, F. A Study of Anomalous Temperature-Programmed Reduction Profiles of Cu_2O, CuO, and CuO−ZnO Catalysts. *J. Catal.* **1994**, *148* (2), 709−721.
(79) Ash-Kurlander, U.; Martin, O.; Fontana, L. D.; Patil, V. R.; Bernegger, M.; Mondelli, C.; Pérez-Ramírez, J.; Steinfeld, A. Impact of Daily Startup−Shutdown Conditions on the Production of Solar Methanol over a Commercial Cu−ZnO−Al_2O_3 Catalyst. *Energy Technology* **2016**, *4* (5), 565−572.
(80) Schulte, M. L.; Truttmann, V.; Doronkin, D. E.; Baumgarten, L.; Nicolai, A.; Beltran, D. A. M.; Summ, F. J.; Kiener, C.; Warmuth, L.; Pitter, S.; et al. Monitoring the Fate of Zn in the Cu/ZnO/ZrO_2 Catalyst During CO_2-to-Methanol Synthesis at High Conversions by *Operando* Spectroscopy. *Angew. Chem., Int. Ed.* **2025**, *64* (15), e202423281.
(81) Gaikwad, R.; Reymond, H.; Phongprueksathat, N.; von Rohr, P. R.; Urakawa, A. From CO or CO_2?: space-resolved insights into high-pressure CO_2 hydrogenation to methanol over Cu/ZnO/Al_2O_3. *Catalysis Science & Technology* **2020**, *10* (9), 2763−2768.
(82) Jurado A, D. A.; Higham, M. D.; Poh, Y. R.; Catlow, C. R. A.; Krossing, I. Mechanism of CO_2 Conversion to Methanol on a Highly Representative Model Cu/ZnO Interface. *J. Catal.* **2025**, *446*, 115997.

https://doi.org/10.1021/acs.energyfuels.5c03664
Energy Fuels 2025, 39, 22342−22355